River Flow 2010 - Dittrich, Koll, Aberle & Geisenhainer (eds) - © 2010 Bundesanstalt für Wasserbau ISBN 978-3-939230-00-7

An investigation of scale effects in the flow past a vertical wall abutment

M. Koken
Civil and Environmental Engineering Department, The University of Iowa, Iowa City, Iowa, USA and Civil Engineering Department, Middle East Technical University, Ankara, Turkey

G. Constantinescu
Civil and Environmental Engineering Department, The University of Iowa, Iowa City, Iowa, USA

ABSTRACT: The physics of the flow past a vertical-wall abutment is investigated using Detached Eddy Simulation (DES) at a high channel Reynolds number, $Re=5*10^5$ (case HR). The study considers conditions corresponding to the start of the scour process (flat bed channel). Scale effects are investigated by comparing the results of the DES simulation with those from a Large Eddy Simulation performed at a much lower Reynolds number, Re=18,000 (case LR). Results from the two simulations show that the size of the region of high amplification of the non-dimensional turbulence kinetic energy within the horseshoe vortex (HV) system decreases with the increase in the Reynolds number. An additional DES simulation ($Re=2.4*10^5$) past an abutment with sloped walls shows that the structure of the HV system and the turbulence amplification in the same region does not depend strongly on the shape of the abutment. The degree of deformation of the cores of the vortex tubes shed in the upstream part of the separated shear layer (SSL) originating at the tip of the abutment was much larger in case HR compared to case LR. This provided an additional mechanism for the amplification of the horizontal vorticity in the near-bed region. Large-scale hairpin-like structures formed in the downstream part of the SSL. The legs of these vortices were oriented parallel to the interface between the high-speed outer flow and the recirculating flow past the obstruction. The lower leg of some of these hairpin vortices was situated, at times, at a small distance from the bed and was able to strongly amplify the local bed shear stress values. Consequently, the bed shear stress distribution in the instantaneous flow fields displayed a streaky structure over part of the SSL region. Due to the richer eddy content of the SSL, the intensity of the non-dimensional pressure r.m.s. fluctuations beneath the SSL was found to be about two times larger in case HR compared to case LR.

Keywords: Numerical Simulations, Coherent Structures, Bridge abutment

1 INTRODUCTION

Bridge abutments are hydraulic structures build out from the river bank. The presence of a bridge abutment in an alluvial channel induces the formation of a scour hole around its base. The dynamics of the large-scale coherent structures controls to a large degree the geomorphodynamic processes around bridge piers and bridge abutments (Sumer & Fredsoe, 2002, Roulund et al., 2005, Fael et al., 2006, Unger and Hager, 2007, Kirkil et al., 2008, Koken & Constantinescu, 2008a-b). The main vortical systems in the flow are the horseshoe vortex (HV) system near the upstream base of the abutment, the recirculating flow region upstream of the abutment, the separated shear layer (SSL) originating at the extremity of the abutment, and the wake flow past the abutment. The unsteady necklace vortices that form the HV system follow the junction line between the bed and the upstream face of the abutment. Downstream of it, these vortices are stretched and bend in the direction of the incoming flow. Because of the presence and interaction among the large-scale coherent structures, large shear stresses and pressure fluctuations at the bed can be induced in some regions situated around the abutment. This generates local scour.

Koken and Constantinescu (2008a, 2008b) provide the first in-depth discussion of the structure and unsteady dynamics of the HV system forming at the base of a vertical abutment wall with flat and deformed scoured bed based on results from Large Eddy Simulation (LES) and dye visualization experiments. Despite the fact that their numerical investigation was conducted at a channel Reynolds number of only 18,000, the structure of the HV system was found to resemble

the one observed in previous investigations of junction flows conducted at much higher Reynolds numbers. In particular, they found that the core of the main necklace vortex is subject to bi-modal aperiodical oscillations with characteristics that are similar to those observed by Devenport and Simpson (1990) in their pioneering experimental study of the HV system forming at the base of a wing-shaped cylinder in a flat-bed channel at Re~$1.15*10^5$ (the length scale in the definition of the Reynolds number is the maximum thickness of the wing). The presence of large-scale self-induced aperiodic oscillations explained why the turbulence (e.g., turbulent kinetic energy, turbulence energy production and Reynolds stresses) levels within the HV system region were about one order of magnitude higher compared to the levels in the incoming turbulent boundary layer. Koken and Constantinescu (2008b) also found that the core of the main necklace vortex continues to be subject to bi-modal aperiodic oscillations as the loose bed evolves between conditions at the initiation of scour (flat bed) and at the end of the scour process (equilibrium deformed bed). The effect of the development of the scour hole was to gradually reduce the amplitude of the large-scale aperiodic oscillations.

Eddy-resolving methods like LES are much more successful to predict massively separated flows compared to RANS methods. Hybrid RANS-LES techniques like Detached Eddy Simulation (DES) can resolve the dynamically most important eddies in the flow and allow studying the dynamics of the coherent structures at Reynolds numbers that are comparable to those encountered in the field (e.g., Kirkil et al., 2009, Kirkil and Constantinescu, 2009). DES uses the same base turbulence model in the RANS and LES regions. No special treatment is required to match the solutions at the boundary between the LES and RANS regions.

The main goal of the present paper is to study the scale effects and thus to try to understand to what extent the findings from relatively low-Reynolds-number (Re~10^4) experimental or LES studies are relevant for practical applications of junction flows in river engineering in which the Reynolds numbers are much higher (Re>10^5). The simulations at the higher Reynolds numbers are performed using DES. Scale effects for the flow past a vertical wall abutment are discussed based on comparison of DES (case HR) with results from an LES simulation at Re=18,000 (case LR) performed by Koken and Constantinescu (2008a). In both simulations the incoming flow contained resolved fluctuations and the ratio between the width of the obstruction, W, and the channel depth, D, was the same (W/D=1.5). Additionally, the effect of the shape of the abutment on the structure of the HV system is investigated by comparing case HR with a similar DES simulation of the flow past an abutment with sloped walls at Re=$2.4*10^5$ (case HR-SW) that is closer to the typical shape of a bridge abutment.

2 NUMERICAL METHOD AND DESCRIPTION OF THE SIMULATIONS

A general description of the DES code is given in Chang et al. (2007). The 3D incompressible Navier-Stokes equations are integrated using a fully-implicit fractional-step method. The governing equations are transformed to generalized curvilinear coordinates on a non-staggered grid. Convective terms in the momentum equations are discretized using a blend of fifth-order accurate upwind biased scheme and second-order central scheme. All other terms in the momentum and pressure-Poisson equations are approximated using second-order central differences. The discrete momentum (predictor step) and turbulence model equations are integrated in pseudo-time using alternate direction implicit (ADI) approximate factorization scheme. In the present DES simulation, the Spalart-Allmaras (SA) one-equation model was used. Time integration in the DES code is done using a double time-stepping algorithm and local time stepping is used to accelerate the convergence at each physical time step. The time discretization is second order accurate.

The geometry of the computational domain in case HR is shown in Fig. 1. The length scale is selected to be the flow depth (D). The mean velocity in the main channel (U) is used as the velocity scale. The abutment length is 1.5D and is located at a distance of 8D from the inflow section. The physical time is 0.02D/U. The geometry of the abutment in case HR-SW can be inferred from Fig. 3. The computational domain is meshed using 7.5 million cells in the DES simulations.

At the inflow section, turbulent inflow conditions corresponding to fully-developed turbulent channel flow are applied. The velocity fields from a preliminary periodic-channel LES simulation at Re=18,000 are stored in a file and then fed in a time-accurate manner through the inflow section in the simulations containing the abutment. The mean streamwise velocity profile at Re=240,000 is obtained from a preliminary RANS simulation and the turbulent fluctuations at Re=18,000 are superimposed on the mean profile. At the outflow, a convective boundary condition is used. The free surface is treated as a rigid lid which is justified as the channel Froude number is 0.2 in experiment. The walls are treated as no-slip boundaries.

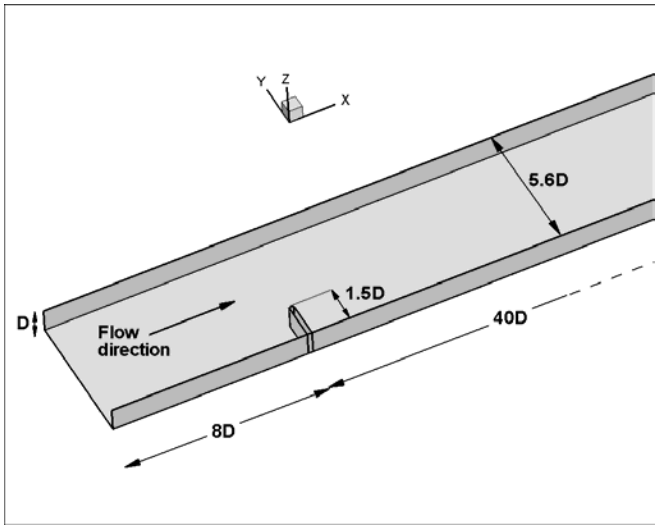

Figure 1: Computational domain in the HR simulation

3 ANALYSYS OF SCALE AND ABUTMENT SHAPE EFFECTS

The Q criterion is used in Fig. 2 to visualize the HV system in the mean flow in the HR and LR cases. At both Reynolds numbers, the cores of the main (HV1) and secondary (HV2) necklace vortices are initially parallel to the upstream face of the vertical wall abutment and then follow the shape of the SSL. In case HR, the legs of HV1 and HV2 merge at some distance downstream of the abutment. On the other hand, HV1 and HV2 remain separated in the LR simulation. Also, in the HR simulation the coherence of HV2 is larger and the circulation of HV1 is more than twice that of HV2 in vertical sections that are perpendicular to the axis of HV1 and are situated between the sidewall and the abutment tip. However, in sections situated past the abutment, the circulation of HV1 decreases rather sharply, while that of HV2 remains approximately constant. In sections situated close to the merging region, the circulation of HV1 is only 20% higher than that of HV2. By comparison, in the LR simulation the circulation of HV2 is less than one third that of HV1 in all vertical sections cutting through the axes of HV1 and HV2.

Though the size and coherence of HV1 are subject to large temporal variations, in average the main necklace vortex is more stable in case HR compared to case LR. In the case of an abutment with a sloped wall (Fig. 3), HV1 extends over a larger distance downstream of the abutment. Its core is larger, however its strength is lower compared to case HR because the adverse pressure gradients induced by the abutment are weaker in case HR-SW. Its positions relative to the abutment and the SSL are similar to the other cases but, in contrast to case HR, the secondary vortex in the mean flow is very weak.

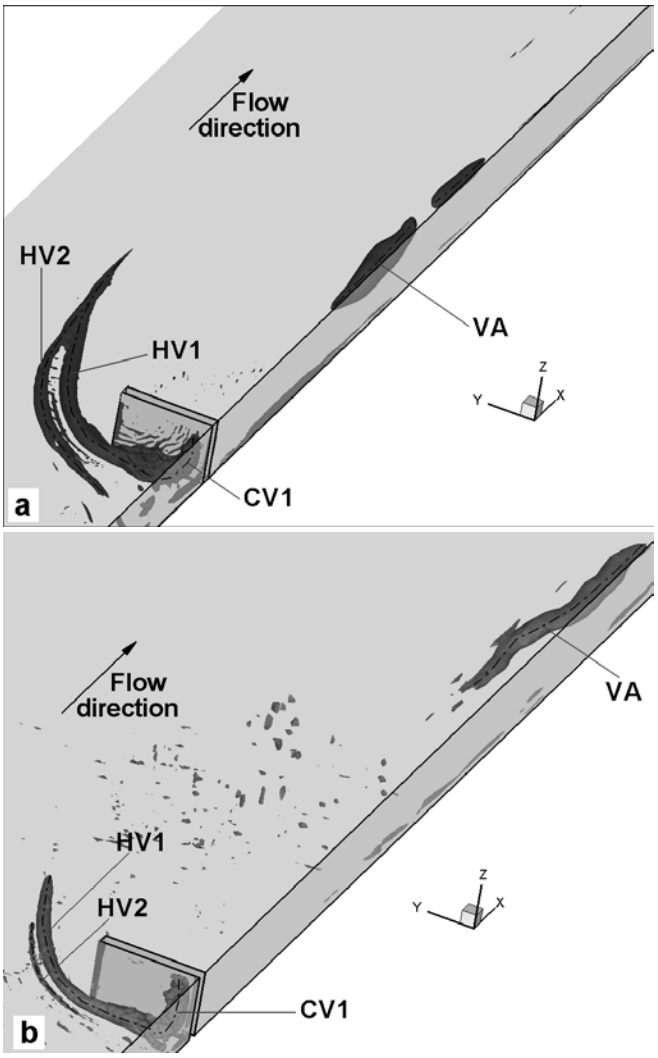

Figure 2: Vortical structure of the mean flow close to the abutment. The eddies are educed using the Q criterion. a) case HR; b) case LR.

Figures 4 and 5 show the distributions of the resolved TKE and pressure r.m.s. fluctuations, p'^2, along with the 2D mean-velocity streamline patterns at a representative vertical section cutting through the region where the strength of the HV system is high for cases HR and HR-SW, respectively. Consistent with previous experimental and numerical investigation of junction flows (e.g., see Simpson, 2001), the pressure and velocity fluctuations are strongly amplified inside the region where the core of HV1 undergoes large-scale oscillations between two preferred states (modes). The levels of amplification of the TKE and p'^2 can be as much as 30 times higher than the levels corresponding to the background turbulence. By comparison, present results for all the three cases show that the amplification of the turbu-

lence inside the core of HV2 above the levels associated with the incoming fully turbulent channel flow is not significant. This suggests that the core of HV2 does not undergo large-scale oscillations.

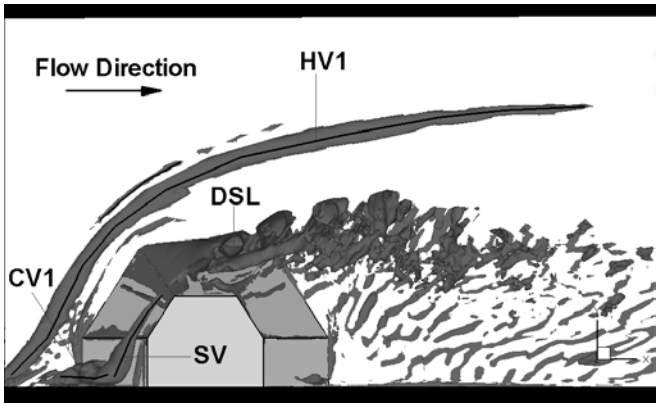

Figure 3: Vortical structure of the mean flow close to the abutment in case HR-SW. The eddies are educed using the Q criterion.

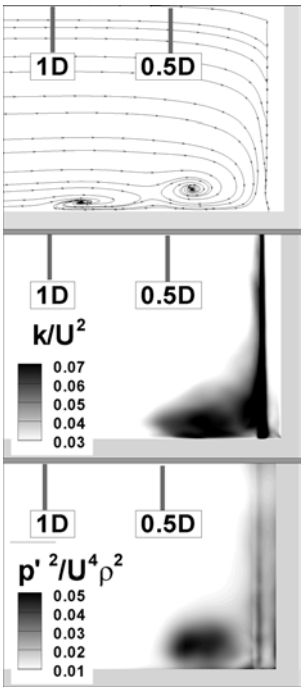

Figure 4: 2D mean flow streamline patterns, nondimensional TKE, k/U^2, and pressure r.m.s. fluctuations, $\overline{p'^2}/(\rho^2 U^4)$, in a vertical sections cutting through the tip of the abutment for case HR.

Examination of the instantaneous flow fields show that the flow in the HV region switches aperiodically between two extreme states that are similar to the zero-flow mode and the back-flow mode described for the first time by Devenport and Simpson (1990). Figure 6 shows the instantaneous velocity vectors in a plane cutting through the tip of the obstruction at two time instants when HV1 is in the zero-flow mode and the back-flow mode for case HR. When a high-momentum irrotational patch of fluid (i.e., coming from the free-surface) reaches the upstream face of the vertical-wall abutment, it is transported toward the bottom with the downflow. As it interacts with the bottom of the channel, the patch tries to preserve its irrotationality and forms a strong near-wall jet in the reverse flow direction. This wall jet pushes HV1 away from the abutment. As a result, the core of HV1 assumes a more elliptical shape, leading to the back-flow mode (Fig. 6b). The other extreme situation (zero-flow mode) occurs when a patch of highly rotational and relatively low-momentum fluid convected from the separating incoming boundary layer reaches the obstruction. In this case separation of the near wall jet occurs earlier, the core of HV1 has a smaller size and is situated closer to the abutment (Fig. 6a). Though some differences are observed in terms of the occurrence and location of the weak recirculation regions upstream of HV1 between cases HR (Fig. 6) and LR (Fig. 7) and the wall jets in both modes are less strong in case HR, the fundamental mechanism associated with the switching between the two modes remains the same.

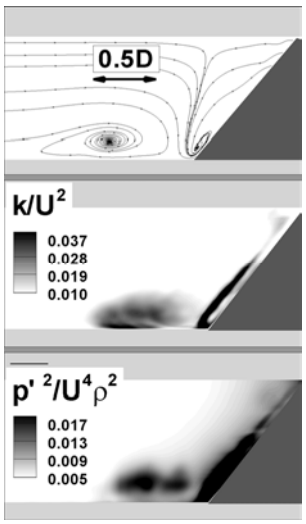

Figure 5: 2D mean flow streamline patterns, nondimensional TKE, k/U2, and pressure r.m.s. fluctuations, $\overline{p'^2}/(\rho^2 U^4)$, in a vertical sections cutting through the tip of the abutment for case HR-SW.

The TKE distributions are qualitatively very similar in all three simulations. As shown in Figs. 4 and 5 for cases HR and HR-SW, two regions of high TKE amplification induced by the bi-modal oscillations of HV1 are present. The first one is situated close to the bed and is due to the variations in the extent and strength of the wall jet forming beneath HV1 (e.g., compare Figs. 6a and 6b). The second one is associated with the changes in the position of the core of HV1. The presence of these two regions of high TKE amplification in sections where the strength of the bi-modal oscillations is high was also observed in the measurements of Devenport and Simpson (1990) in the symmetry

plane of the flow past a wing-shaped cylinder. The thin band of high TKE extending over most of the channel depth corresponds to the SSL.

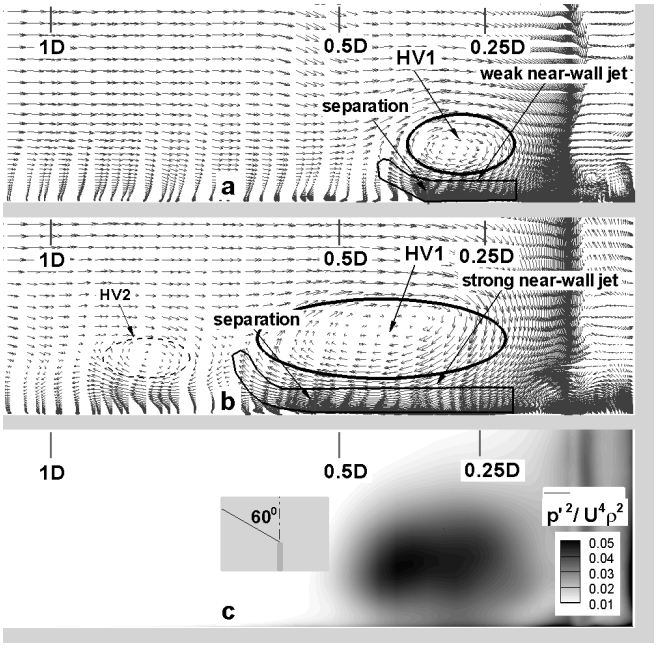

Figure 6: Instantaneous velocity vectors in a plane cutting through the tip of the abutment (see inset in frame c) showing HV1 in the zero-flow mode (frame a) and the back-flow mode (frame b) for case HR. Frame c shows the distribution of the pressure r.m.s. fluctuations, $\overline{p'^2}/(\rho^2 U^4)$.

In all the three simulations a double-peak distribution is observed at all vertical sections where the amplitude of the bi-modal oscillations was sufficiently high such that the regions of large p'^2 values associated with each mode did not merge into a single patch of elliptical shape. The smaller amplitude of the large scale oscillations of HV1, together with the fact that the core of HV1 was smaller and more stable in case HR, explain the less clear separation between the two regions of high p'^2 in Figs. 4 and 6c compared to Fig. 7c for case LR and Fig. 5 for case HR-SW.

Next, we focus on the analysis of the changes in the structure of the SSL with the Reynolds number. As shown in Fig. 8, the eddies populating the SSL are more irregular in case HR, in particular over the lower part of the channel ($z/D<0.3$) where most of the vortex tubes are strongly deformed, starting in the formation region. This is clearly observed by comparing Figs. 8a (case HR) and 8b (case LR). In the HR simulation the core of the second vortex tube is strongly deformed in the vertical direction. As a result, the vorticity vector inside the vortex tube reorients in a direction that makes a relatively low angle with the bed. Through this mechanism additional horizontal vorticity is induced in the near-bed region. This has obvious consequences on the sediment entrainment phenomena beneath the SSL. As one moves downstream, the growth of secondary instabilities is very rapid, such that at a distance of 1.5D from the obstruction large-scale eddies are connecting the distorted cores of the vortex tubes. By comparison, the cores of the vortex tubes remain close to vertical in case LR.

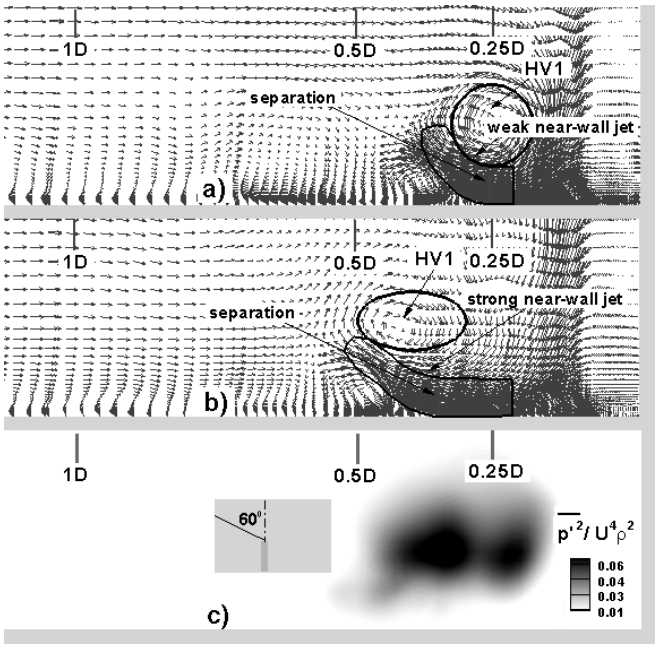

Figure 7: Instantaneous velocity vectors in a plane cutting through the tip of the abutment (see inset in frame c) showing HV1 in the zero-flow mode (frame a) and the back-flow mode (frame b) for case LR. Frame c shows the distribution of the pressure r.m.s. fluctuations, $\overline{p'^2}/(\rho^2 U^4)$.

As shown in Figs. 8c and 8d, large-scale hairpin-like eddies are observed at several locations inside the SSL, in the HR simulation. However, the two legs of the hairpins are not contained in a plane parallel to the bed, as expected to happen if these coherent structures would form as a result of the interaction of the incoming turbulent flow with the bed. Rather, the legs of the hairpins are contained in a plane that is close to vertical. The large-scale hairpin structures form as a result of the growth of secondary instabilities associated with the transition between the high-speed flow on the outward side of the SSL and the low-speed flow inside the main recirculation region in the wake. The hairpins are contained mostly inside the SSL and the high-speed flow side. The presence of large-scale hairpin structures in the transition region (shear layer) between a high-speed stream of fluid and a low-speed region was also observed in flow past cavities (e.g., see Chang et al., 2006) and at the interface between a high Reynolds number lock-exchange gravity current and the surrounding flow. At some locations, the vorticity levels in the legs of the hairpin structures are comparable to those in the vortex tubes. In particular, examination of the instantaneous flow

fields show that the lower leg is situated, at times, at small distances from the bed and can induce large bed-shear-stress values.

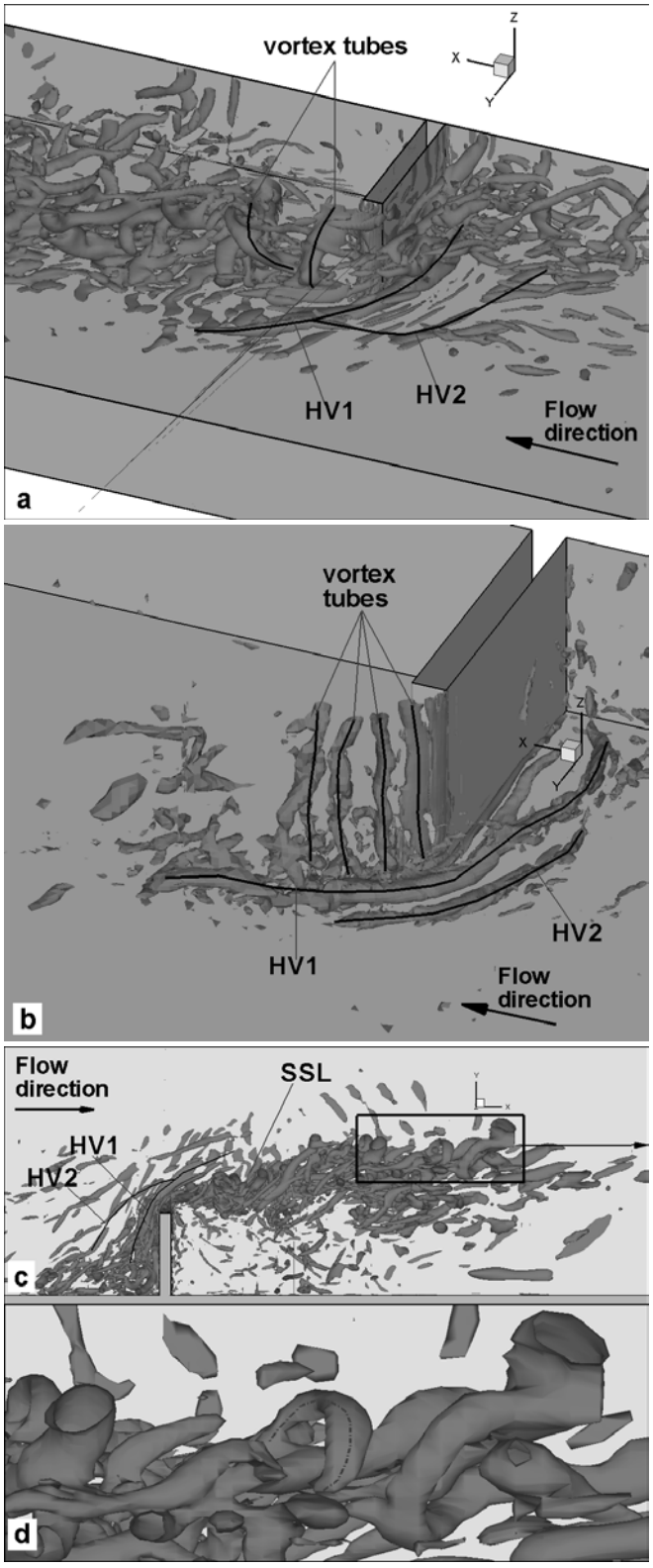

Figure 8: Visualization of vortical structure of the instantaneous flow using the Q criterion. a) General view (case HR); b) General view (case LR); c) Top view (case HR); d) Detail view showing the presence of hairpin-like structures in the SSL (case HR).

Figure 9a visualizes the distribution of the bed friction velocity, u_τ/U, for case HR at an arbitrary time instant. Based on the Shields diagram, the threshold value for sediment entrainment for a sediment size of d_{50}=1.05 mm is $u_{\tau c0}/U$=0.056. This is the typical sediment size employed in loose-bed experiments performed in the flume that was used to study local scour development for the flow conditions considered in case HR. The regions where sediment is expected to be entrained due only to large values of the bed friction velocity ($u_\tau > u_{\tau c0}$) are delimited in Fig. 9a using a solid line. The presence of relatively high pressure fluctuations at the bed may produce sediment entrainment even if $u_\tau < u_{\tau c0}$.

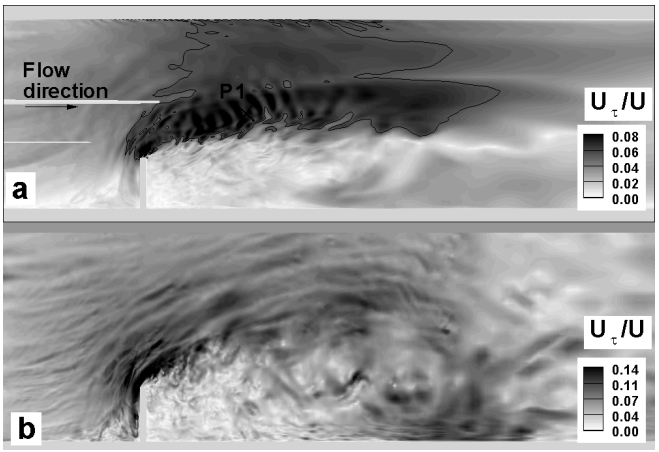

Figure 9: Distribution of bed-friction velocity. a) Instantaneous flow, case HR; b) Instantaneous flow (case LR). The solid contour line in frame (a) corresponds to $u_{\tau c0}/U$=0.056.

The largest values of u_τ (~0.07-0.1U) in the mean and instantaneous flow fields occur beneath the upstream part of the SSL and the main necklace vortex. One should stress that an important contribution to the magnitude of the friction velocity in the region situated around the tip of the abutment comes from the amplification of the near-bed velocity due to the acceleration of the flow as it passes the obstruction, rather than to the presence of HV1. Similar to case LR, the bed friction velocity beneath the upstream part of HV1 remains lower than $u_{\tau c0}$.

The distribution of u_τ in case HR (Fig. 9a) shows the presence of streaks of high bed friction velocity beneath the SSL region in the instantaneous flow. The primary reason for the formation of these streaks is the presence of hairpin-like structures in the vicinity of the bed (see discussion of Fig. 8). The amplification of u_τ inside these streaks can be important, up to two times the mean value of u_τ at the same location. In the upstream part of the SSL (distances less than 1D from the tip of the obstruction), it is the passage of the vortex tubes that is mainly responsible for the local amplification of u_τ. Figure 9b shows the distribution of u_τ in the instantaneous flow for case LR. Consistent with the eddy content of the SSL in the LR simulation (no hairpin-like structures

are present in Fig. 8b), no streaks of high u_τ values are observed beneath the downstream part of the SSL.

The other main factor that determines the capacity of the flow to entrain sediment particles from the bed is the level of the pressure r.m.s. fluctuations. The distribution of $p'^2/(\rho^2 U^4)$ at the bed is plotted in Fig. 10 for cases LR and HR. In both simulations, p'^2 is large around the tip of the abutment and beneath the SSL. Observe also the relatively high p'^2 values around the region where the flow reattaches to the sidewall (x/D~13) and, in particular, the amplification of p'^2 beneath the core of the elongated junction vortex VA forming close to the sidewall containing the abutment (Fig. 3). Though the distributions are qualitatively similar, the non-dimensional p'^2 levels are, in average, two times larger in the HR simulation. This increase is explained by the richer eddy content of the SSL, especially in the near-bed region.

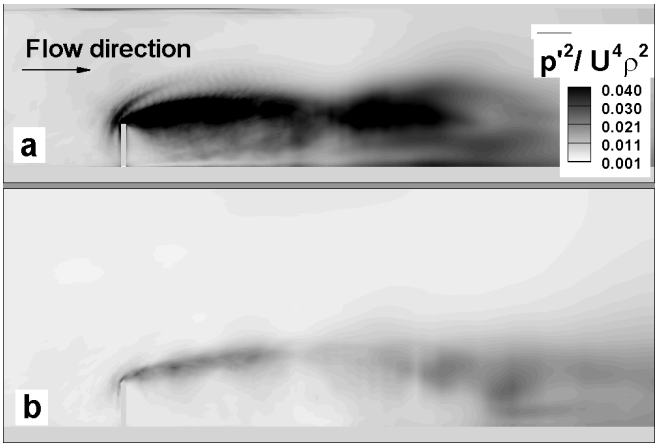

Figure 10: Distribution of the pressure r.m.s. fluctuations at the bed, $\overline{p'^2}/(\rho^2 U^4)$. a) case HR; b) case LR.

4 SUMMARY AND CONCLUSIONS

The present study used DES to investigate the changes in the flow and turbulence structure around an abutment mounted at one of the sidewalls of a long straight channel due to changes in the Reynolds number and the shape of the abutment. The quantification of scale effects is of great interest as many experimental studies of junction flows that are relevant for environmental engineering and, in particular, of local scour studies are conducted in laboratory flumes at Reynolds numbers that are much lower than those encountered in the field. Not accounting properly for scale effects in scour prediction methods can result in the severe overprediction of maximum scour depth (Ettema et al., 1998). Changes in the Reynolds number can induce both qualitative and quantitative changes in the structure of the large-scale coherent structures that control the local scour around the flow structure (e.g., abutment).

The structure and dynamics of the HV system in the two simulations were found to be qualitatively similar. The core of the main necklace vortex HV1 was shown to undergo bimodal aperiodic oscillations, similar to the ones observed in experimental investigations of other junction flows. The intensity of the bimodal oscillations was found to peak at sections cutting through the tip of the abutment, where the overall amplification of the turbulence intensity (e.g., TKE and pressure r.m.s. fluctuations) was the highest. The bimodal oscillations gradually disappeared in the leg of HV1. As a result of the increase in the Reynolds number, the main necklace vortex became more stable, the size of its core decreased, and the average amplitude of the aperiodic oscillations got lower. The non-dimensional pressure r.m.s. fluctuations at the bed were significantly stronger beneath the HV region, and the non-dimensional TKE values inside the HV system were 20-40% smaller in the HR simulation compared to the LR simulation.

A main finding of this study is that the eddy content of the SSL changes considerably between the two Reynolds numbers. The degree of deformation of the cores of the vortex tubes in the upstream part of the SSL was much larger in the HR simulation. This provided an additional mechanism for the amplification of the horizontal vorticity in the near-bed region. Additionally, the secondary instabilities acting on the cores of the vortex tubes were much stronger in the HR simulation. Large scale hairpin-like eddies formed in the downstream part of the SSL. The legs of these vortices were oriented parallel to the interface between the high speed outer flow and the recirculating flow behind the obstruction. The lower leg of some of these hairpin vortices was situated, at times, at a small distance from the bed and was able to strongly amplify the bed-shear-stress. Consequently, in the HR simulation the bed shear stress distribution in the instantaneous flow fields displayed a streaky structure over part of the SSL region. Similar to the LR simulation, the largest values of the bed shear stress occurred in the strong acceleration region around the tip of the obstruction, and beneath the main necklace vortex and the upstream part of the SSL. The overall non-dimensional levels of the bed shear stress in the instantaneous and mean flow were smaller in the HR simulation. This is consistent with the expected decrease of the non-dimensional bed shear stress with the increase of the Reynolds number in fully developed turbulent channel flows.

Due to the richer eddy content of the SSL in the HR simulation, the values of the non-dimensional pressure r.m.s. fluctuations beneath the SSL were found to be around two times larger in the HR simulation compared to the LR simulation. This means that flume experiments conducted at relatively low Reynolds numbers substantially underestimate the effect of the pressure fluctuations on sediment entrainment.

Finally, the presence of an obstacle of a shape that better approximates that of most bridge abutments did not result in important qualitative changes in the structure of the HV system and the dynamics of these vortices. However, the sloped walls induced lower adverse pressure gradients that resulted in a weaker downflow and a weaker, but larger size, main necklace vortex. The distribution of the TKE and pressure rms fluctuations inside the HV region remained similar. The coherence of the secondary necklace vortex was very low for the abutment with sloped walls. This resembled more the HV system observed in case LR rather than case HR.

The present study considered only scale and abutment shape effects at conditions corresponding to the start of the scour process (no local scour, flat bed channel). A similar investigation is under way for conditions in which a large scour hole is present around the abutment.

ACKNOWLEDGEMENTS

The authors would like to thank the National Center for High Performance Computing (NCHC) in Taiwan for providing the computational resources needed to perform some of the simulations as part of the collaboration program between NCHC and IIHR-Hydroscience and Engineering. Additional computer support was provided by the TRACC facility at the Argonne National Laboratory.

REFERENCES

Chang, K., Constantinescu, G., Park, S.O. 2007. Assessment of predictive capabilities of Detached Eddy Simulation to simulate flow and mass transport past open cavities. ASME J. Fluids Engineering, 129(11), 1372-1383.

Chang, K.S., Constantinescu, S. G., Park, S. 2006. "Analysis of the flow and mass transfer processes for the incompressible flow past an open cavity with a laminar and fully turbulent incoming boundary layer, J. Fluid Mech., 561, 113-145.

Devenport, W. J., Simpson, R. L. 1990. Time-dependent and time-averaged turbulence structure near the nose of a wing-body junction. J. Fluid Mech., 210, 23-55.

Ettema, R., Melville, B. W., Barkdoll, B. 1998. Scale effects in pier-scour experiments. J. Hydraulic Engineering, 124(6), 639-642.

Fael, C. M. S., Simarro-Grande, G., Martin-Vide, J. P.,, Cardoso, A. H. 2006. Local scour at vertical-wall abutments under clear water flow conditions. Water Resources Research, 42, W10408, doi:10.1029/2005WR004443.

Kirkil, G., Constantinescu, G., Ettema, R. 2009. DES investigation of turbulence and sediment transport at a circular pier with scour hole. J. Hydraulic Engineering, 135(11), 888-901.

Kirkil, G., Constantinescu, G. 2009. Nature of flow and turbulence structure around an in-stream vertical plate in a shallow channel and the implications for sediment erosion. Water Resources Research, 45, W06412, doi:10.1029/2008WR007363.

Koken, M., Constantinescu, G. 2008a. An investigation of the flow and scour mechanisms around isolated spur dikes in a shallow open channel. Part I. Conditions corresponding to the initiation of the erosion and deposition process. Water Resources Research, 44, W08406, doi:10.1029/2007WR006489.

Koken, M., Constantinescu, G. 2008b. An investigation of the flow and scour mechanisms around isolated spur dikes in a shallow open channel. Part II. Conditions corresponding to the final stages of the erosion and deposition process. Water Resources Research, 44, W08407, doi:10.1029/2007WR006491.

Roulund, A., Sumer, B. M., Fredsoe, J., Michelsen, J. 2005. Numerical and experimental investigation of flow and scour around a circular pile. J. Fluid Mechanics, 534, 351-401.

Sumer, B. M., Fredsoe J. 2002. The mechanics of scour in the marine environment. World Scientific.

Unger, J., Hager, W.H. 2007. Downflow and horseshoe vortex characteristics of sediment embedded bridge piers. Experiments in Fluids, 42(1), 1-19 DOI 10.2007/s00348-006-0209-7.